AGU100 ADVANCING EARTH AND SPACE SCIENCE

JGR Oceans

Key Points:
- Warmer ocean surface produces stronger storms and leads to higher storm surge throughout Chesapeake Bay
- Sea level rise has a moderate effect on storm surge height
- Hardening shorelines significantly increase storm surge height in the middle and upper parts of the Bay

Supporting Information:
- Supporting Information S1

Correspondence to:
F. Zhang,
fzhang@umces.edu

Impacts of Ocean Warming, Sea Level Rise, and Coastline Management on Storm Surge in a Semienclosed Bay

Fan Zhang[1] and **Ming Li[1]**

[1]Horn Point Lab, University of Maryland Center for Environmental Science, Cambridge, MD, USA

Abstract Regional atmosphere and ocean models are used to investigate how sea level rise, ocean warming, and coastline management affect storm surge in the semienclosed Chesapeake Bay. Using Hurricane Isabel (2003) as a case study, the storm is placed under the climatic conditions projected for 2050 and 2100. Higher sea surface temperature increases the latent heat release from the ocean, resulting in large increases in storm intensity and maximum sustained wind speeds. The storm surge height, defined as the difference between storm tide and astronomical tide, is amplified in the future climate and amounts to ~30% of the relative sea level rise. Hardening shorelines further increases the storm surge height in the middle and upper parts of the Bay by up to 0.5 m. Sea level rise has a modest impact on the storm surge height: decreasing it by 0.1–0.2 m if the low-lying areas are allowed to be flooded but increases it by 0.1–0.3 m if hypothetic walls are placed at the current coastline. Ocean warming is the main driver of storm surge amplification in the future climate. Energy budget analysis shows that allowing flooding over low-lying areas leads to a significant energy loss and reduces the storm surge height in the estuary.

1. Introduction

U.S. coasts have a number of semienclosed bays and estuaries. Their enclosed reaches can increase their vulnerability to storm surge during tropical cyclones with tracks resulting in up-estuary winds (Boicourt, 2005). For instance, Hurricane Isabel (2003) moved on the west side of Chesapeake Bay after landfall, creating historical flooding in Washington, DC, Baltimore, and rural areas on the eastern shore of Chesapeake Bay (Li et al., 2006). Similarly, Hurricane Sandy's (2012) track crossed the New Jersey coastline at a nearly 90° angle and generated record-setting flooding in New York City (Lin et al., 2012). Climate change is expected to increase the rate of sea level rise (Intergovernmental Panel on Climate Change [IPCC], 2013; Church et al., 2013) and cause significant increases in extreme weather such as tropical storms (Eichler et al., 2013; Emanuel et al., 2008; Knutson et al., 2013; Woollings et al., 2012). It will likely exacerbate storm surge and coastal flooding in bays and estuaries, but its effects need to be better understood and quantified.

The global sea level rise rate was ~1.6 mm/year in the second half of 20th century (Domingues et al., 2008) and is accelerating in the 21st century. Under the highest emission scenario of IPCC AR5 (Fifth Assessment Report of the Intergovernmental Panel on Climate Change), the projected global mean sea level rise is 0.52–0.98 m by the end of 21st century (Church et al., 2013). Some parts of the ocean rise faster than others. Tide-gauge records in Chesapeake Bay show that sea levels increased by 3–5 mm/year over the twentieth century, twice that of the global average (Zervas, 2009). Land subsidence was a dominant contributor to the high relative sea level rise (Miller et al., 2013). Changing ocean circulation and accelerated regional warming may also contribute to higher sea levels in coastal regions (Domingues et al., 2018; Ezer, 2013; Ezer et al., 2013; Sallenger et al., 2012). According to recent probabilistic projections (Kopp et al., 2014, 2017), the likely range (66% chance) of relative sea level rise in Chesapeake Bay over the 21st century is 0.6 to 1.3 m, up to 4 times of the sea level rise experienced during the past century (Boesch et al., 2018).

How will climate change affect tropical cyclones in the future? Most studies based on coarse-resolution general circulation models (GCMs) have shown that warmer climate will increase the intensity and decrease the frequency of tropical cyclones (Bengtsson et al., 2007). On the other hand, Vecchi and Soden (2007) found that vertical wind shear will increase considerably with warming, leading to reduced tropical cyclone activity. Using an ensemble of GCMs and scenarios from Phases 3 and 5 of the Coupled Model Intercomparison Project (CMIP3 and CMIP5), Knutson et al. (2013) conducted dynamic downscaling projections of the 21st

century Atlantic hurricane activity. They found over 20% reductions in the overall tropical storm frequency but 40–80% increases in the frequency of severe hurricanes across all models. On the other hand, Emanuel (2013) found increases in both frequency and intensity of storms during the 21st century under the highest emission scenario.

Several studies have investigated the impact of sea level rise and climate change on storm surge in coastal regions. Smith et al. (2010) found that sea level rise may greatly amplify surge heights in shallow wetland areas of southeast Louisiana. Yang et al. (2014) found that the response of storm surge to land subsidence and sea level rise at the northern coasts of the Gulf of Mexico is highly nonlinear and varies spatially and temporally. Using an empirical formula to link hurricane intensity change to ocean warming, Mousavi et al. (2011) examined the combined effects of sea level rise and warming on storm surge in Corpus Christi, Texas, and projected that the hurricane flood elevation will on average rise by 0.8 m by 2080s. Lin et al. (2012) showed that changing storm climatology in concert with 1-m sea level rise may increase the probability of present New York City 100-year surge flooding by over 5 times by the end of 21st century. When changes in storm climate is considered, Lin et al. (2016) found that Hurricane Sandy's flooding frequency at New York City significantly increases over 21st century compared to the scenario with sea level rise alone.

Similar questions must be addressed for Chesapeake Bay. Hurricane Isabel (2003) generated widespread flooding over the Chesapeake Bay region (Li et al., 2006, 2007; Shen et al., 2006; Zhong et al., 2010) and is considered as a 100-year flooding event for planning purposes by cities and towns around Chesapeake Bay. A major open question is how much more flooding such a storm might generate in 2050 or 2100 when the mean sea level and ocean temperature are higher. Another major question is how coastal communities might respond to the flooding risk and whether coastline management affects storm surge response in the semienclosed Bay. One coastline option might be to build sea walls, levees, and other gray infrastructure at the coastline to protect against flooding. Another coastline option might be to make use of salt marshes, sea grasses, and other green infrastructure to mitigate flooding risk. In a recent modeling study of Chesapeake and Delaware Bays, Lee et al. (2017) found that the response of tidal ranges to sea level rise depends critically on the coastline management. Tidal range increases if hypothetic sea walls are built at the current coastline to prevent flooding but decreases if low-lying land is allowed to be flooded. Similar results were found in modeling studies of tidal response to sea level rise and coastline management on the European shelf (Pelling et al., 2013; Pickering et al., 2012; Ward et al., 2012) and in San Francisco Bay (Holleman & Stacey, 2014; Wang et al., 2017).

In this paper we investigate the impacts of sea level rise, ocean warming, and coastline management on storm surge in Chesapeake Bay. Regional atmosphere and ocean models are used to simulate Hurricane Isabel (2003) and Isabel-like storms in the future climate as projected by the global climate models. The regional atmosphere model can explicitly simulate the effects of warmer ocean temperature on storm intensity while the regional ocean model will directly simulate the effects of sea level rise on water levels. To investigate how coastline management might affect storm surge response inside Chesapeake Bay, we will simulate two shoreline scenarios: (1) the hard shoreline scenario in which hypothetic walls are placed at the current coastline to prevent flooding and (2) the soft shoreline scenario in which low-lying land areas are allowed to be flooded. The outline of this paper is as follows. Section 2 describes the modeling approach, and section 3 presents the model projections for storm surge in 2050 and 2100. The relative effects of sea level rise and ocean warming on storm surge are examined in section 4. An energy budget analysis is presented in section 5 to explain different storm surge responses in the future climate, particularly how the storm surge differs between the soft and hard shorelines.

2. Method

To investigate how climate change and coastline management affect storm surge in Chesapeake Bay, we used regional atmosphere and ocean models. The regional atmosphere model, based on Weather Research and Forecasting (WRF) model, simulates the impact of ocean warming on storm intensity. The regional ocean model, based on Finite Volume Community Ocean Model (FVCOM), simulates the impact of sea level rise, changing storm intensity and coastline management on storm surge.

2.1. Regional Atmospheric Model

The Advanced Research WRF model is a nonhydrostatic, mesoscale atmospheric model (Version 3.6.1; Skamarock et al., 2008) and has been widely used for hurricane simulations (e.g., Li & Pu, 2008; Nolan, Zhang, et al., 2009,Nolan, Stern, et al., 2009; Seroka et al., 2016). In this study, triple-nested model domains were configured for WRF (Figure 1a). The outermost domain has a resolution of 12 km and covers the western Atlantic. The middle domain covers the south and middle Atlantic regions at a resolution of 4 km. The innermost domain uses a fine resolution of 1.33 km to resolve the Chesapeake Bay region. There are 40 vertical sigma levels. At the lateral boundaries of the 12-km domain, WRF is forced by the 1° Final (FNL) operational global analysis data (https://rda.ucar.edu/datasets/ds083.2/). At the ocean surface, WRF is forced by daily outputs from 0.5° real-time global sea surface temperature (RTG-SST, http://polar.ncep.noaa.gov/sst/). FNL is also used to initialize WRF at 2 days prior to the landfall of hurricane. We used commonly used parameterization schemes for the subgrid-scale physics in the WRF model (Zhang et al., 2017). The Thompson scheme is used for cloud microphysics (Thompson et al., 2008), the rapid radiative transfer model is used for the shortwave and longwave radiations (Iacono et al., 2008), the Yonsei University scheme is used for planetary boundary layer (Hong et al., 2006), the Kain-Fritsch scheme is used for cumulus parameterization in the 12-km resolution domain (Kain, 2004), and the MM5 similarity is used for the surface layer (Fairall et al., 2003).

2.2. Regional Ocean Model

The unstructured-grid FVCOM (Chen et al., 2003, 2006) has been used for storm surge and inundation simulations (e.g., Beardsley et al., 2013; Chen et al., 2013; Weisberg & Zheng, 2006). Our model domain covers Chesapeake Bay and eastern U.S. continental shelf, as shown in Figure 1b (Zhang et al., 2017). The horizontal grid sizes are ~10 km near the open ocean boundary, ~1 km on the inner shelf, and ~200 m inside Chesapeake Bay. To simulate overland inundation, finer resolutions (10–200 m) are placed over the low-lying land areas surrounding Chesapeake Bay (up to 5-m height above the current mean sea level; Figure 1c). The bathymetry and land elevation data were from National Oceanic and Atmospheric Administration and U.S. Geological Survey, respectively. A detailed description of bathymetry, digital elevation, and datum used in the FVCOM can be found in Lee et al. (2017).

The model is run in a three-dimensional barotropic mode. Five evenly distributed sigma layers are used in the vertical direction, but temperature and salinity are kept constant. At the open boundary, 10 tidal constituents (M_2, S_2, N_2, K_2, K_1, O_1, P_1, Q_1, M_m, and M_f) are prescribed with global tidal model TOPEX/POSEIDON 7.1 (Egbert & Erofeeva, 2002). At the ocean surface, FVCOM is forced by hourly winds from WRF. At the ocean bottom, a quadratic stress is applied, assuming a logarithmic bottom boundary layer. The bottom roughness height is set to be 1 cm in Chesapeake Bay and 2 cm on the adjacent shelf (Lee et al., 2017). The vertical eddy viscosity and diffusivity are computed using the k-ε turbulence closure scheme (Burchard, 2002; Warner et al., 2005), and the background diffusivity and viscosity are set to be 10^{-5} and 5×10^{-6} m^2/s, respectively. FVCOM was initialized at 6 days prior to the landfall in order to give sufficient time for the model to spin up.

2.3. Design of Numerical Experiments

To project the impact of climate change on storm surge and coastal inundation in 2050 and 2100, we made use of the IPCC AR5 (Fifth Assessment Report). IPCC AR5 provides a set of four pathways of global greenhouse gas emission scenarios called Representative Concentration Pathways (RCPs; Moss et al., 2010; Van Vuuren et al., 2011). We selected two RCPs in our modeling analysis: stabilized emissions (RCP 4.5) and growing emissions (RCP 8.5).

CMIP5 (Coupled Model Intercomparison Project Phase 5) used in the IPCC AR5 contains a large ensemble of GCMs among which 15 widely used GCMs were used in this study (Table S1 in the supporting information). We extracted SST in the tropical North Atlantic Ocean from these GCMs and calculated the averaged SST difference between the future climate (2046–2065 for "2050" and 2081–2100 for "2100") and the historical reference period 1986–2005. Then, the GCMs with minimum, median, and maximum SST changes were selected for the downscaling simulations. The median projection is for SST to increase by 1.13/1.71 °C at 2050 and by 1.48/2.94 °C at 2100, corresponding to projections from RCP 4.5/RCP 8.5 (Table 1). The inter model spread in SST is larger in 2100 than in 2050, reflecting larger uncertainty in the projection for the end of 21st century.
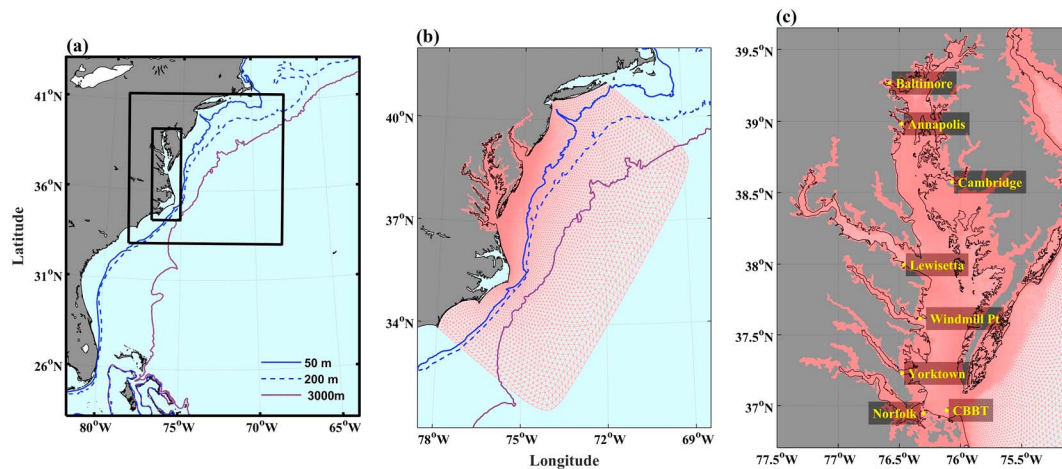
Figure 1. (a) Triple-nested Weather Research and Forecasting model domains (thick black boxes) with resolution of 12, 4, and 1.33 km. (b) Finite Volume Community Ocean Model grids (red). (c) Zoomed-in view of Finite Volume Community Ocean Model grids over Chesapeake Bay and the surrounding coastal plains.

The GCMs were also used to project sea level rise. Church et al. (2013) analyzed individual contributions to sea level rise and estimated the median values and likely ranges for projections of global mean sea level in the 21st century relative to 1986–2005. The relative sea level rise rate in Chesapeake Bay is larger than the global mean rate due to land subsidence (Zervas, 2001, 2009) and changing ocean dynamics in the northwest Atlantic Ocean (Ezer, 2013; Ezer et al., 2013; Sallenger et al., 2012). The regional land subsidence due to glacial isostatic adjustment was estimated following Miller et al. (2013). The regional sea level rise due to changing ocean dynamics was estimated according to Yin et al. (2009). Adding the three components together yielded the relative sea level rise in 2050 and 2100 (Table 1). To account for the relative sea rise in FVCOM, the projected increase in the mean sea level was uniformly superimposed onto the astronomical tides along the open boundary of FVCOM. Forcing the sea level rise projections at the offshore boundary produces essentially the same results as more elaborate modeling approaches in which land subsidence is accounted for through bathymetry changes (Bilskie et al., 2016; Lee et al., 2017).

To examine how different coastline management options might affect storm surge in a changing climate, we considered two shoreline options. In the soft shoreline approach, flooding to the low-lying coastal plains is allowed. A point treatment technique is adopted by FVCOM: a grid is treated as a wet/dry point when the

Table 1
Projected Increases in SST in The tropical North Atlantic Ocean and Relative Sea Level Rise in Chesapeake Bay

	RCP 4.5			RCP 8.5		
2050	median	minimum	maximum	median	minimum	maximum
SST increase in tropical North Atlantic (°C)	1.13	0.83	2.11	1.71	1.20	2.64
Global mean sea level rise	0.26	0.19	0.33	0.30	0.22	0.38
Regional ocean dynamics	0.09	0.07	0.10	0.09	0.07	0.10
Regional land subsidence	0.075	0.065	0.085	0.075	0.065	0.085
Relative sea level rise (m)	0.43	0.33	0.52	0.47	0.36	0.57
2100						
SST increase in tropical North Atlantic (°C)	1.48	0.98	2.54	2.94	2.30	4.24
Global mean sea level rise	0.53	0.36	0.71	0.74	0.52	0.98
Regional ocean dynamics	0.17	0.13	0.19	0.17	0.13	0.19
Regional land subsidence	0.15	0.13	0.17	0.15	0.13	0.17
Relative sea level rise (m)	0.85	0.62	1.07	1.06	0.78	1.34

Note. The "median," "minimum," and "maximum" projections are based on the median value and likely lower and upper bounds of the projected global mean sea level rise in the IPCC AR5 report. SST = sea surface temperature; IPCC AR5 = Fifth Assessment Report of the Intergovernmental Panel on Climate Change; RCP = Representative Concentration Pathways.

water depth is higher/lower than h_c (5 cm in our model; Chen et al., 2011). In the hard shoreline approach, hypothetical sea walls are built along the current coastline and no overland inundation was allowed, following a similar approach by Pelling et al. (2013) and Lee et al. (2017).

We conducted a total of 25 numerical experiments: one hindcast simulation of Hurricane Isabel (2003) which served as the baseline for the comparison and 12 simulations of future storms each for soft or hard shoreline scenarios (Table S2). For the hindcast, WRF was forced by the FNL data at the lateral boundary and by daily RTG-SST at the ocean surface. For Isabel-like storms in 2050 and 2100, WRF and FVCOM considered the effects of warming and sea level rise under the median, lower and upper range projections from RCP 4.5 and 8.5. The projected SST increases in 2050 and 2100 were added to the historical RTG-SST to set the ocean surface boundary condition for WRF. Following the approach of Hill and Lackmann (2011) and Mallard et al. (2013), the GCM-projected changes in the atmosphere temperature between the historical period and future climate were averaged horizontally over the tropical Atlantic Ocean and then added to the FNL outputs to set the initial and lateral boundary conditions for WRF (Figures S1 and S2). Tropic relative humidity showed relatively little changes between the current and future climate in the GCMs and were thus not considered (see also Hill & Lackmann, 2011; Shen et al., 2000). Neither did we take into account of the changes in wind fields because of the larger uncertainty in wind prediction in the GCMs. This study focuses on the storm surge in the semienclosed Chesapeake Bay, and adding GCMs-projected wind changes to FNL led to storm tracks further away from the estuary. Our approach provides a cost-effective alternative to running high-resolution regional climate models (Knutson et al., 2013) and captures changes in the atmospheric thermal conditions (temperature and moisture) associated with warmer SST. It focuses on the thermodynamic component of climate change and its effects on tropic storms, and does not consider changes in the vertical wind shear (Tuleya et al., 2016).

3. Changes in Storm Intensity and Storm Surge

In this section we present results from the WRF-FVCOM simulations of Hurricane Isabel and Isabel-like storms in the future climate. Our analysis will focus on storm surge, but the total water level will also be studied.

3.1. Storm Intensity

Hurricane Isabel traveled northwestward and made landfall at the Outer Bank of North Carolina on 18 September 2003. WRF captured the storm track well, with the root-mean-square error between the predicted and observed tracks at 29.3 km (Figure 2a). WRF also accurately modeled the forward propagation speed, with the observed and predicted time stamps nearly at the same locations. The observed minimum sea level pressure (MSLP) reached a low of 953 mb on 17 September but increased to 1,000 mb on 19 September. The predicted MSLP time series was in good agreement with the observations (Figure 2b). Isabel attained a maximum sustained wind (MSW) of 45 m/s prior to landfall, which was well simulated by WRF (Figure 2c).

When exposed to warmer SST, storm intensifies. By 2050 MSLP decreases to a minimum of 942–953 mb under RCP 4.5 and 938–952 mb under RCP 8.5, with a larger range of the projected values under RCP 8.5 (Figure 2b). Maximum MSW increases to ~56–63 m/s under RCP 4.5 and ~56–61 m/s under RCP 8.5 (Figure 2c). By 2100 MSLP decreases to a minimum of ~941–952 mb under RCP 4.5 and ~930–943 mb under RCP 8.5 (Figure 2e). MSW also becomes stronger in the future climate: increasing from a peak speed of 55 m/s during Isabel to ~56–60 m/s under RCP 4.5 and ~59–65 m/s under RCP 8.5 (Figure 2f). Overall, the increase of storm intensity from 2050 to 2100 is modest under RCP 4.5 but significant under RCP 8.5. Since the same large-scale atmospheric flow fields were used to force WRF at the lateral boundary, the storm in the future climate follows essentially the same track as Hurricane Isabel (Figures 2a and 2d). However, it moves at a slightly lower speed, with the forward propagation speed decreasing from 8.3 m/s during Isabel to ~7.8 m/s in 2050 and ~7.3 m/s in 2100 under the climate change scenario RCP 8.5.

The storm intensification is driven by larger heat release from the ocean surface (Figures 3a and 3b). The maximum latent heat flux around the eyewall was ~640 W/m^2 during Isabel but increases 12% to 715 W/m^2 in 2100 under the median projection of RCP 8.5. This is associated with 2.94 °C increase in SST (Table 1). In Figure 3c we plot the time series of the averaged latent heat flux over a 200-km radius of the storm center for Hurricane Isabel as well as its cousins in the future climate. The area-averaged heat flux
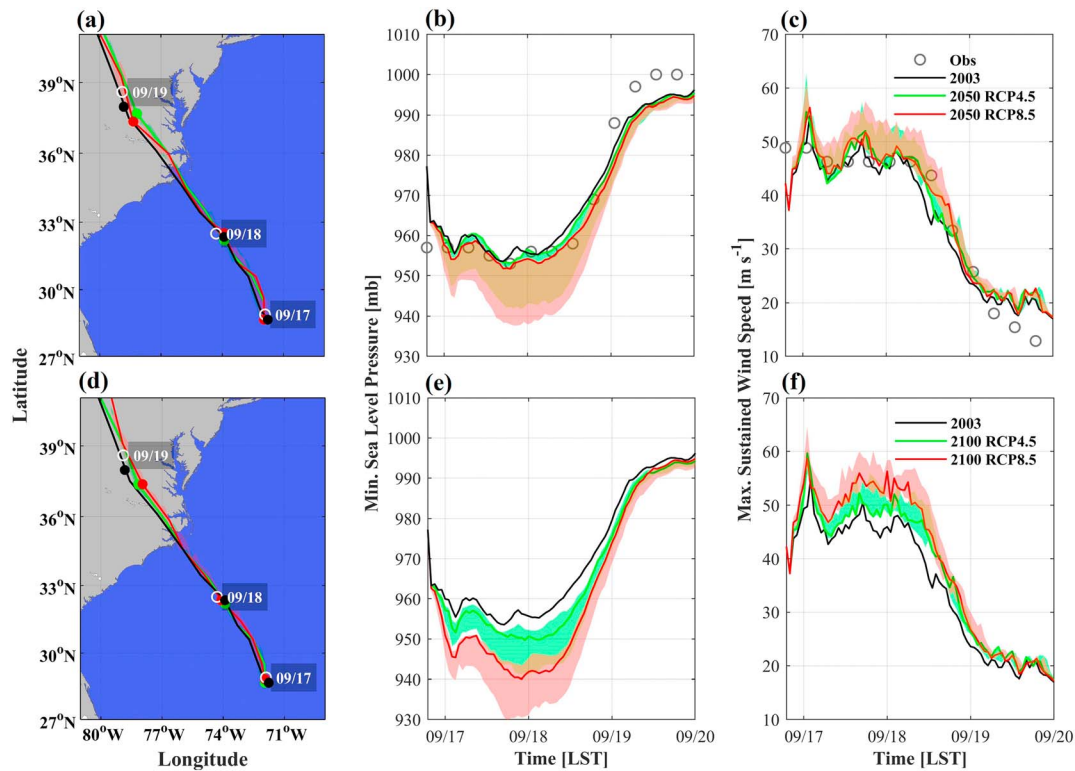
Figure 2. (a) Storm tracks, time series of (b) minimum sea level pressure, and (c) maximum sustained wind speed for Hurricane Isabel (black) and similar storms in 2050 (green and red). (d)–(f) The same as (a)–(c) but for Isabel-like storms in 2100. The white circles in (a) and (d) indicate the observed track. The thick green and red lines represent results from "median" projection for the SST increase and the shaded area are bounded by the minimum and maximum values from "min," median, and "max" projections. RCP = Representative Concentration Pathway.

was around 450–550 W/m^2 before Isabel's landfall. It increases to 480–600 W/m^2 in 2050 and 500–680 W/m^2 in 2100. To show the connection between the latent heat flux and ocean temperature more clearly, we calculated the time average Q_L of the area-averaged heat flux between 0000 LST 17 September and the landfall, and plotted it against the SST increase (ΔSST) for all the storms simulated by WRF. Q_L increases linearly with ΔSST, at a rate of 38 W·m^{-2}·°C^{-1} (Figure 3d). On the other hand, the minimum value of MSLP decreases almost linearly with ΔSST: 1 °C warming increases the central pressure deficit by ~9% (Figure 3d). Knutson and Tuleya (2004, 2008) found a similar linear relationship between hurricane intensity change and SST increase.

3.2. Storm Surge

Stronger storms drive higher storm surge in the future climate, but there are regional differences in the surge response. To focus on the surge height, the mean sea level rise and tidal signals were removed from sea level time series by subtracting sea levels from tide-only runs with corresponding sea level increase and shoreline configuration (Figure 4). We compared the storm surge at three locations: Norfolk, VA, Cambridge, MD, and Baltimore, MD, representative of the lower, middle, and upper Bay regions. The soft shoreline scenario is considered first but will be compared with the hard shoreline scenario in section 3.3. Storm surge at Norfolk rose to a maximum of 1.88 m during Hurricane Isabel. By 2100, it is projected to rise to 1.97–2.03 m under RCP 4.5 and 2.00–2.22 m under RCP 8.5 (Figure 4a). Similar amplification of the storm surge is seen at Baltimore: increasing from a peak height of 2.24 m during Isabel to 2.25–2.34/2.32–2.44 m under RCP 4.5/8.5 (Figure 4c). These represent 10–20% increases in the surge heights, corresponding to similar increases in the wind speed magnitude (Figure 2f). In contrast, the storm surge in all the model runs reaches a similar or lower height at Cambridge, which is located next to low-lying land areas in the middle Bay that are flooded during the storm. It is noted that the peak storm surge arrives 2–3 hr later in 2100, since the storm forward propagation speed decreases (see Figure 2d).
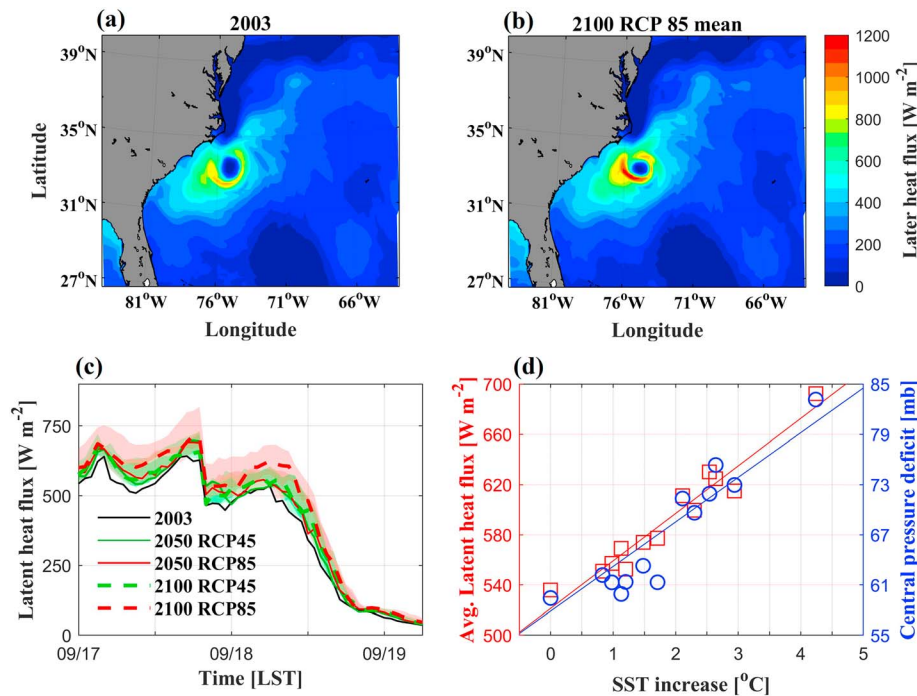
Figure 3. Snapshots of upward surface latent heat flux at 0600 LST 18 September for (a) hindcast and (b) 2100 RCP 8.5 median scenario. (c) Time series of surface latent heat flux for all scenarios. The latent heat flux is averaged over the area within 200 km of the storm center. (d) Relationship between time-averaged latent heat flux (red) /central pressure deficit (blue) and SST increase. Latent heat flux is averaged between 17 September and landfall. RCP = Representative Concentration Pathway; SST = sea surface temperature.

Next we compare storm surge across the entire estuary. In all the model runs, the surge height displays a similar longitudinal distribution (Figures 5a and 5b). It is large in the lower Bay due to proximity to the storm center as well as incoming surge wave generated on the shelf. As the storm moves further away from the Bay, however, the surge height decreases between the lower and middle Bay. It increases again in the upper Bay because southwesterly winds on the right quadrants of the storm push water toward the head of the estuary. The surge height is projected to increase in the future climate, with larger changes under RCP 8.5 than under RCP 4.5. By the end of 21st century, the peak surge at the lower Bay stations can be 0.4–0.6 m higher, which is ~50% of the projected relative sea level rise.

In terms of coastal inundation, the total water level is a more relevant metric. In Figures 6a–6e, we plot the spatial distribution of the peak water level over Chesapeake Bay generated by Hurricane Isabel and its future cousins. Part of the water level increase is associated with the relative sea level rise which is projected to be 0.43/0.47 m in 2050 and 0.85/1.06 m in 2100 under the median projection of RCP 4.5/8.5 (Table 1). However, there are regional variations in the sea level response to climate change. Large peak water level increases are seen in the lower Bay, western tributaries and upper Bay. For example, the peak water level at Baltimore was 2.24 m during Hurricane Isabel but reaches 3.38 m in 2100 under the median projection of RCP 8.5. In contrast, the total water level increases by about the same amount as the mean sea level rise in the middle Bay. Low-lying areas on the eastern shore of Chesapeake Bay (at latitudes between 38°N and 38.5°N) are flooded by the storm, such that the storm water moves across the land rather than being confined by the coastline.

3.3. Impact of Coastline Management on Storm Surge

The storm surge generated inside the semienclosed Bay is also affected by the manner how the coastline is managed. Here we present model results from the hard shoreline scenario in which sea walls are built at the current coastline to prevent flooding over low-lying coastal plains. The median projections of RCP 4.5 and 8.5 for 2100 are used for comparing the storm surge between the two shoreline scenarios. Norfolk is located near the mouth of Chesapeake Bay, and the surge height there is thus least affected by the coastline management inside the estuary (Figure 4d). At the middle Bay location (Cambridge), the storm surge is appreciably
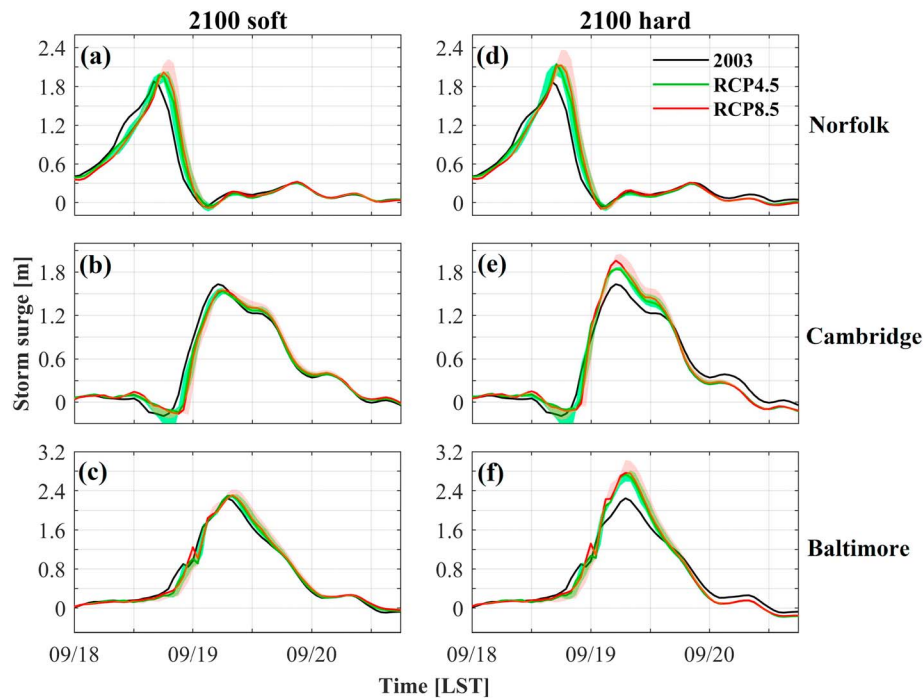
Figure 4. Time series of storm surge at Norfolk, Cambridge, and Baltimore under different scenarios in 2100. The solid green and red lines are from the median projection of each climate change scenario, and the shaded area are bounded by the minimum and maximum values from "min," "median," and "max" scenarios. RCP = Representative Concentration Pathway.

higher in the model run with the hard shoreline: the peak surge height reaches 1.96 m in the hard shoreline versus 1.55 m in the soft shoreline under the median projection of RCP 8.5 (Figure 4e). At the upper Bay location (Baltimore), the differences are even larger (Figure 4f): The surge height reaches 2.76 m in the hard shoreline versus 2.32 m in the soft shoreline. Therefore, how the coastline is managed can result in over 0.4-m difference in the storm surge in an upper Bay location like Baltimore. This is even larger than the surge amplification due to ocean warming or about 40% of the relative sea level rise projected for 2100.

Similar differences between the soft and hard shoreline scenarios are found in the comparison of the peak surge height across the entire estuary (Figure 5). In all the model runs considered, whether for 2050 or 2100 and under RCP 4.5 or RCP 8.5, the surge height is consistently higher under the hard shoreline scenario than under the soft shoreline scenario (cf. Figures 5a and 5b with Figures 5c and 5d). In the lower Bay locations, such as Norfolk and Yorktown, the difference is small. However, it becomes progressively larger as the head of the estuary is approached. In the middle Bay locations south of 38.5°N (Windmill Pt. and Lewisetta), the peak surge height in the hard shoreline exceeds that in the soft shoreline by about 0.10–0.15 m. A significant proportion of the low-lying areas around Chesapeake Bay are located on the eastern shore between 38°N and 38.5°N. North of this region, storm surge responds more strongly to the coastline management. In 2100, the surge height difference between the hard and soft shorelines reaches 0.39 m at Cambridge, 0.41 m at Annapolis, and 0.44 m in Baltimore. This difference is relatively insensitive to the climate change scenario and is about the same under either RCP 4.5 or 8.5. These results have highlighted the potential role of coastline management in altering the storm surge in a semienclosed bay. Hardening shorelines to protect low-lying areas may substantially amplify storm surge in up-estuary locations. We also note that the storm surge height difference between the soft and hard shorelines is larger in 2100 than in 2050, indicating that the influence of shoreline management is magnified in warmer climate.

These differences in storm surge height translate to similarly large differences in the total sea level between two shoreline scenarios (Figure 6). At Baltimore, the peak water level reached 2.24 m during Hurricane Isabel. Under the median projection of RCP 8.5 for 2100, it will reach 3.38 m in the soft shoreline scenario but 3.82 m in the hard shoreline scenario. Thus, the peak water level generated by an Isabel-like storm will be ~70% higher if the shoreline is hardened.
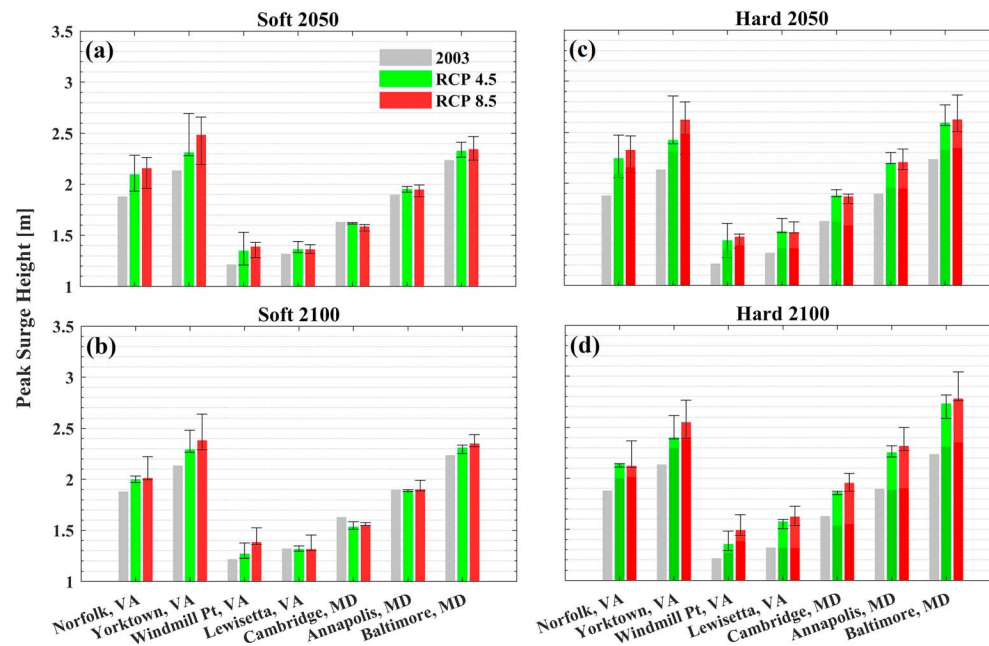
Figure 5. Peak surge heights at seven tidal gauge stations along the main channel of Chesapeake Bay (from left to right on the horizontal axis: from lower Bay to upper Bay) under different scenarios of climate change (Representative Concentration Pathway, RCP 4.5 and 8.5) and coastline management (soft versus hard). The red and green bars represent the median peak surge heights, and the error bars show the range of peak surge heights based on "min," "median," and "max" projections of each climate change scenario. The median peak surge heights in (a) and (b) are also plotted in (c) and (d), respectively, with darker green and red.

4. Effects of Sea Level Rise and Ocean Warming on Storm Surge

To separate the effects of ocean warming and sea level rise on storm surge, we conducted additional model runs for 2100 using the median projection of RCP 8.5: one with SST increase only and another with sea level rise only. In Figure 7, we compare the storm surge time series (mean sea level rise and tidal signals removed) from these two model runs against those from Hurricane Isabel and the full model simulation for 2100 under RCP 8.5. In the model run with soft shoreline and sea level rise only, storm surge is slighted lower in the future climate, with 0.12-m decrease at Norfolk and Cambridge (lower and middle Bay) and 0.14-m decrease at Baltimore (Upper Bay). In the model run with hard shoreline and sea level rise only, storm surge is nearly the same at Norfolk but significantly higher (0.19–0.28 m) at Cambridge and Baltimore. However, these changes are smaller than those seen in the model runs with higher SST only. In the soft shoreline scenario, the storm surge increases by 0.26 m at Norfolk, 0.03 m at Cambridge, and 0.23 m at Baltimore. In the hard shoreline scenario, the storm surge experiences even larger increases: 0.37 m at Norfolk, 0.25 m at Cambridge, and 0.46 m at Baltimore. These model comparisons show that ocean warming is the main driver of storm surge amplification in the future climate. Sea level rise will raise the mean sea level, but its direct effect on the storm surge is relatively small.

To illustrate these effects over the entire Bay, we plot the distribution of the peak surge height (Figure 8). In the model runs forced with the sea level rise only, the surge height decreases by 0.1–0.2 m if the low-lying areas are allowed to be flooded (soft shoreline), but it increases by 0.1–0.3 m if hypothetic walls are placed at the current coastline (hard shoreline; Figures 8a and 8b). These results are similar to what Lee et al. (2017) found in their study of tidal response to sea level rise. The tidal range in Chesapeake and Delaware Bays decreases in the model runs with the soft shoreline but increases in the model run with the hard shoreline.

In the model runs forced with higher SST, storm surge in the estuary is higher in 2100 than 2003, regardless of the coastline management scenario. Stronger winds generate higher storm surge. In the case of soft shoreline, the largest increase occurs in the western tributaries of lower Bay due to its proximity to the storm center, the second largest increase occurs in the upper Bay, whereas moderate to no increases are seen in the middle Bay where low-lying areas on the eastern shore is flooded (Figure 8c). The amplification of the
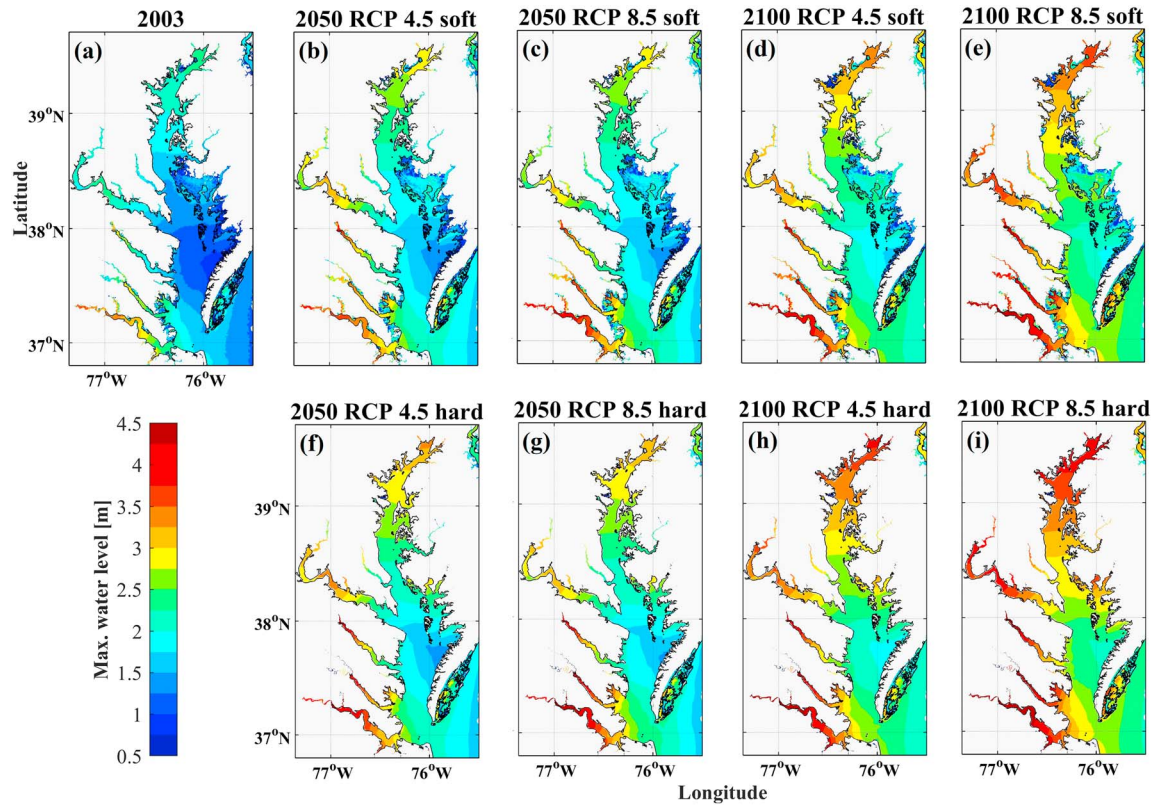
Figure 6. (a–i) Spatial distribution of peak water level from hindcast and future median projection of climate change scenario Representative Concentration Pathway (RCP) 4.5 and 8.5.

storm surge is considerably larger in the case of hard shoreline, especially in the lower and upper Bay regions (Figure 8d). Overall, it is the warming ocean that drives storm surge amplification in the future climate, and hardening shoreline will further amplify the storm surge significantly.

5. Energy Budget Analysis

To better understand the underlying physics of how the storm surge responds to climate change and coastline management, we conducted a diagnostic analysis of the energy budget for storm surge currents. Ignoring the baroclinic effects, the kinetic energy equation (Gill, 1982) can be written as follows:

$$\frac{\partial KE}{\partial t} = -\overrightarrow{\nabla} \cdot \left[\left(p' + KE \right) \overrightarrow{u} \right]$$

$$+ \rho \left[\frac{\partial}{\partial x} \left(\overrightarrow{u} \cdot K_h \frac{\partial \overrightarrow{u}}{\partial x} \right) + \frac{\partial}{\partial y} \left(\overrightarrow{u} \cdot K_h \frac{\partial \overrightarrow{u}}{\partial y} \right) + \frac{\partial}{\partial z} \left(\overrightarrow{u} \cdot K_v \frac{\partial \overrightarrow{u}}{\partial z} \right) \right] - \rho K_h \left[\left(\frac{\partial \overrightarrow{u}}{\partial x} \right)^2 + \left(\frac{\partial \overrightarrow{u}}{\partial y} \right)^2 \right] - \rho K_v \left(\frac{\partial \overrightarrow{u}}{\partial z} \right)^2$$

$$(1)$$

where the kinetic energy $KE = \frac{1}{2} \rho \overrightarrow{u}^2$, ρ is density, $\overrightarrow{\nabla} = \left(\frac{\partial}{\partial x}, \frac{\partial}{\partial y}, \frac{\partial}{\partial z} \right)$, p' is pressure perturbation, $\overrightarrow{u} = (u, v, w)$ is the velocity vector, and K_h and K_v are the horizontal and vertical eddy viscosity, respectively. This equation states the time rate change of the kinetic energy is determined by the divergence of pressure work $(p' \overrightarrow{u})$ and kinetic energy advection $(\overrightarrow{u} KE)$, wind stress/bottom stress work, and energy dissipation. The advective contribution to the energy flux is usually 2 orders of magnitude smaller than the barotropic flux and hence will be neglected (Cummins & Oey, 1997; Zhong & Li, 2006). The horizontal dissipation term is also much smaller than the vertical dissipation term and can be neglected. Then equation (1) can be simplified to the following:
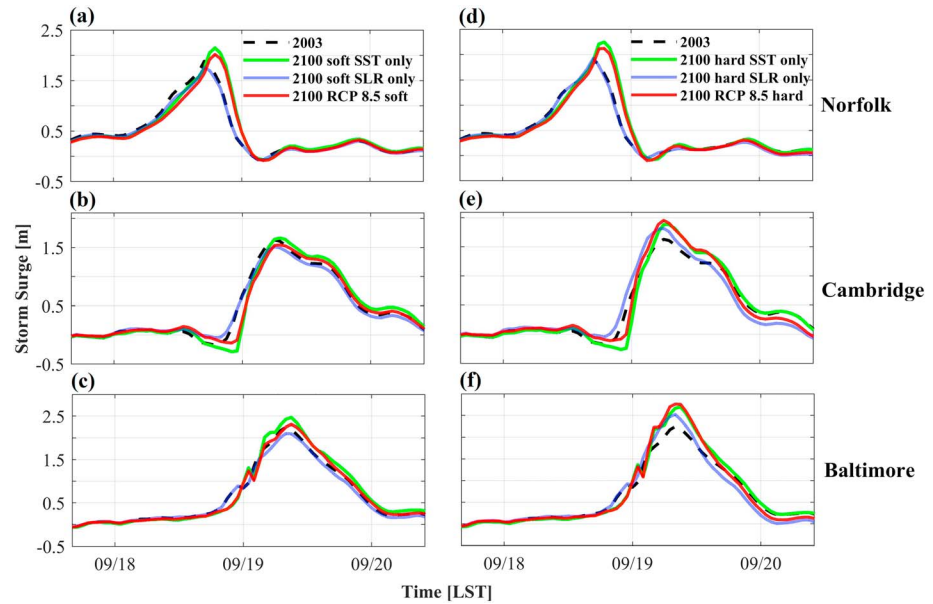
Figure 7. Time series of storm surge at (a) Norfolk, (b) Cambridge, and (c) Baltimore under different soft shoreline scenarios. (d)–(f) The same as (a)–(c) but for hard shoreline scenarios. RCP = Representative Concentration Pathway; SST = sea surface temperature.

$$\frac{\partial KE}{\partial t} = -\overrightarrow{\nabla} \cdot \left(p^{'}\overrightarrow{u}\right) + \rho\frac{\partial}{\partial z}\left(\overrightarrow{u} \cdot K_v \frac{\partial \overrightarrow{u}}{\partial z}\right) - \rho K_v \left(\frac{\partial \overrightarrow{u}}{\partial z}\right)^2 \tag{2}$$

Integrating equation (2) over a control volume (V) yields

$$\underbrace{\iiint_V \frac{\partial KE}{\partial t} \mathrm{d}V}_{\mathrm{d}KE/\mathrm{d}t} = \underbrace{\iint_{S1} p^{'}(u,v) \cdot \overrightarrow{n_1} \mathrm{d}S}_{\text{Incoming flux } (F_{\mathrm{in}})} - \underbrace{\iint_{S2} p^{'}(u,v) \cdot \overrightarrow{n_2} \mathrm{d}S}_{\text{Lateral flux } (F_{\mathrm{lat}})} - \iint_{S3} p^{'} w_0 \mathrm{d}S + \underbrace{\iint_{S3} \overrightarrow{u_s} \cdot \overrightarrow{\tau_s} \mathrm{d}S}_{\text{Wind input } (P_w)} \tag{3}$$
$$+ \iint_{S3} \overrightarrow{u_b} \cdot \overrightarrow{\tau_b} \mathrm{d}S - \underbrace{\iiint_V \rho K_v \left(\frac{\partial \overrightarrow{u}}{\partial z}\right)^2 \mathrm{d}V}_{-\text{dissipation } (\varepsilon)}.$$

The control volume is selected to be the entire Chesapeake Bay bounded by the cross section at the mouth of the estuary ($S1$), the lateral boundary at the current coastline ($S2$), the mean sea level at the surface ($S3$), and the bottom bathymetry ($S4$). In equation (3), $\overrightarrow{n_1}$ and $\overrightarrow{n_2}$ represent the normal vectors perpendicular to $S1$ and $S2$; $\overrightarrow{\tau_s}$ and $\overrightarrow{\tau_b}$ are surface and bottom stress, respectively. Since $p^{'} \cdot w_0 = \rho g \eta \cdot \frac{\partial \eta}{\partial t} = \frac{\partial \frac{1}{2}\rho g \eta^2}{\partial t}$ under the hydrostatic assumption, the third term on the right-hand side can be interpreted as the rate of change in potential energy ($\mathrm{d}PE/\mathrm{d}t$). Rearranging leads to

$$\mathrm{d}E/\mathrm{d}t = F_{\mathrm{in}} - F_{\mathrm{lat}} + P_w - \varepsilon \tag{4}$$

where $\mathrm{d}E/\mathrm{d}t = \mathrm{d}KE/\mathrm{d}t + \mathrm{d}PE/\mathrm{d}t$ is the total energy. The storm surge energy has two source terms: the energy flux across the mouth of the Bay due to incoming storm surge and the local wind energy input due to the action of wind stress on the surface of the Bay. It has two sink terms: the energy flux across the lateral boundary, which is 0 in the presence of hard shoreline but nonzero if water is allowed to flood into the adjacent low-lying land, and the dissipation of energy due to turbulence.

We investigate the energy budget for Hurricane Isabel first. Figure 9a shows the time series of three largest terms in equation (4). Most of the storm surge energy is supplied by the local wind energy input through the surface of the estuary, but the incoming storm surge adds a significant amount of energy input and peaks
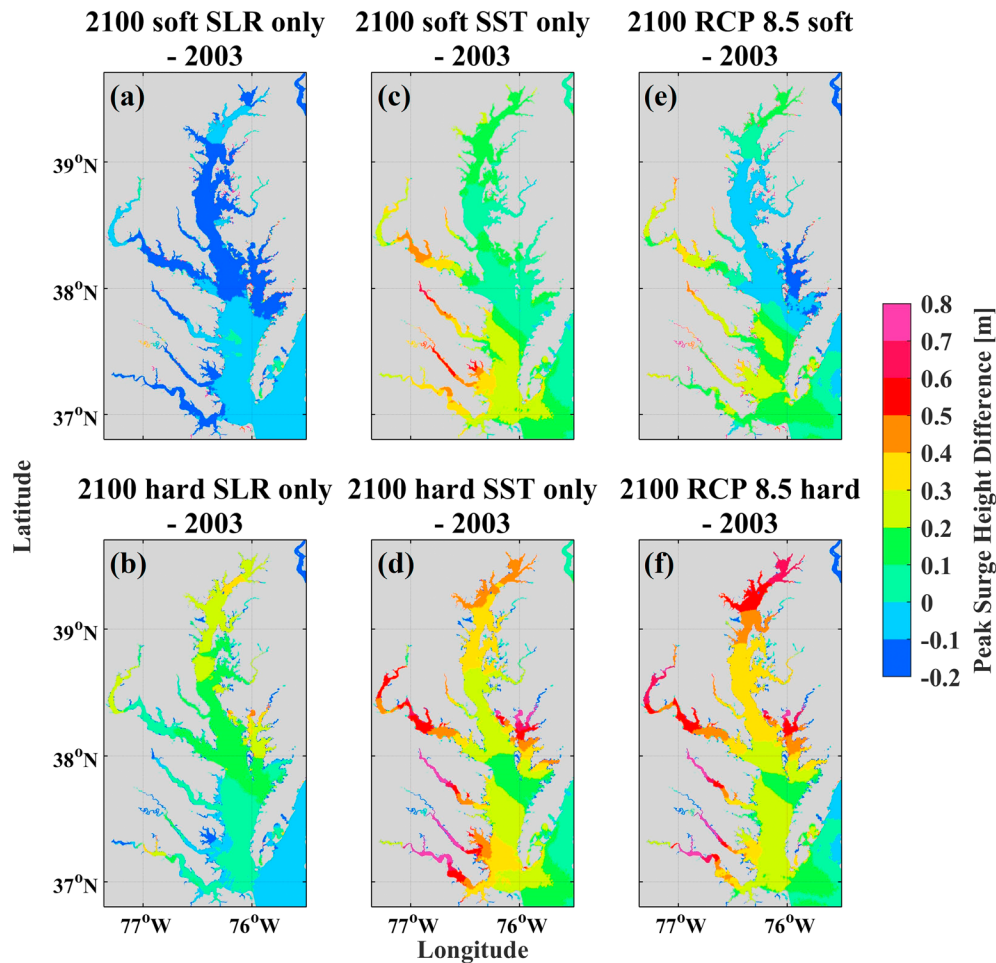
Figure 8. (a, c, and e) Differences in peak surge height between the soft shoreline experiments and hindcast. (b, d, and f) The same as (a), (c), and (e) but for differences between the hard shoreline experiments and hindcast. RCP = Representative Concentration Pathway; SST = sea surface temperature.

earlier than the wind energy input as the storm makes landfall to the south of the Bay and then moves northwestward. Figures 9b and 9c show the spatial distributions of the time-averaged wind energy input and energy dissipation. The energy dissipation approximately balances the wind energy input. In the lower Bay, the dissipation exceeds the wind energy input since the incoming storm surge energy is dissipated there. In the second-order balance of equation (4), we compare the time series F_{in}, F_{lat}, P_w-ε, and dE/dt (Figure 10a). Although F_{lat} is relatively small, it is initially negative as the storm water floods the low-lying areas but becomes positive later as the storm water recedes back to the Bay. The growth of the storm surge energy closely tracks F_{in} during the first half of the storm period since the local wind energy input is only slightly larger the dissipation. In the second half of the storm period, the dissipation exceeds the local wind input and determines the decay of storm surge energy. Figure 10b shows how the total storm surge energy in the Bay varies over time. The integrated energy flux through the lateral boundary is a small but not insignificant loss of the total energy.

Second, we investigate the energy budget for the storm in the median projection of RCP 8.5 in 2100 and with the hard shoreline. The dominant balance is still among the wind energy input, incoming energy flux through the mouth of the estuary, and energy dissipation (Figure 9d). When averaged over the storm period, the horizontal distribution of the energy dissipation shows a broad match with that of wind energy input. In the lower Bay, dissipation clearly exceeds wind energy input as the incoming storm surge energy is dissipated. In the second-order energy balance, $dE/dt > 0$ initially as the energy dissipation ramps up to oppose the wind energy input and the incoming energy flux, and $dE/dt < 0$ later as the incoming energy flux is
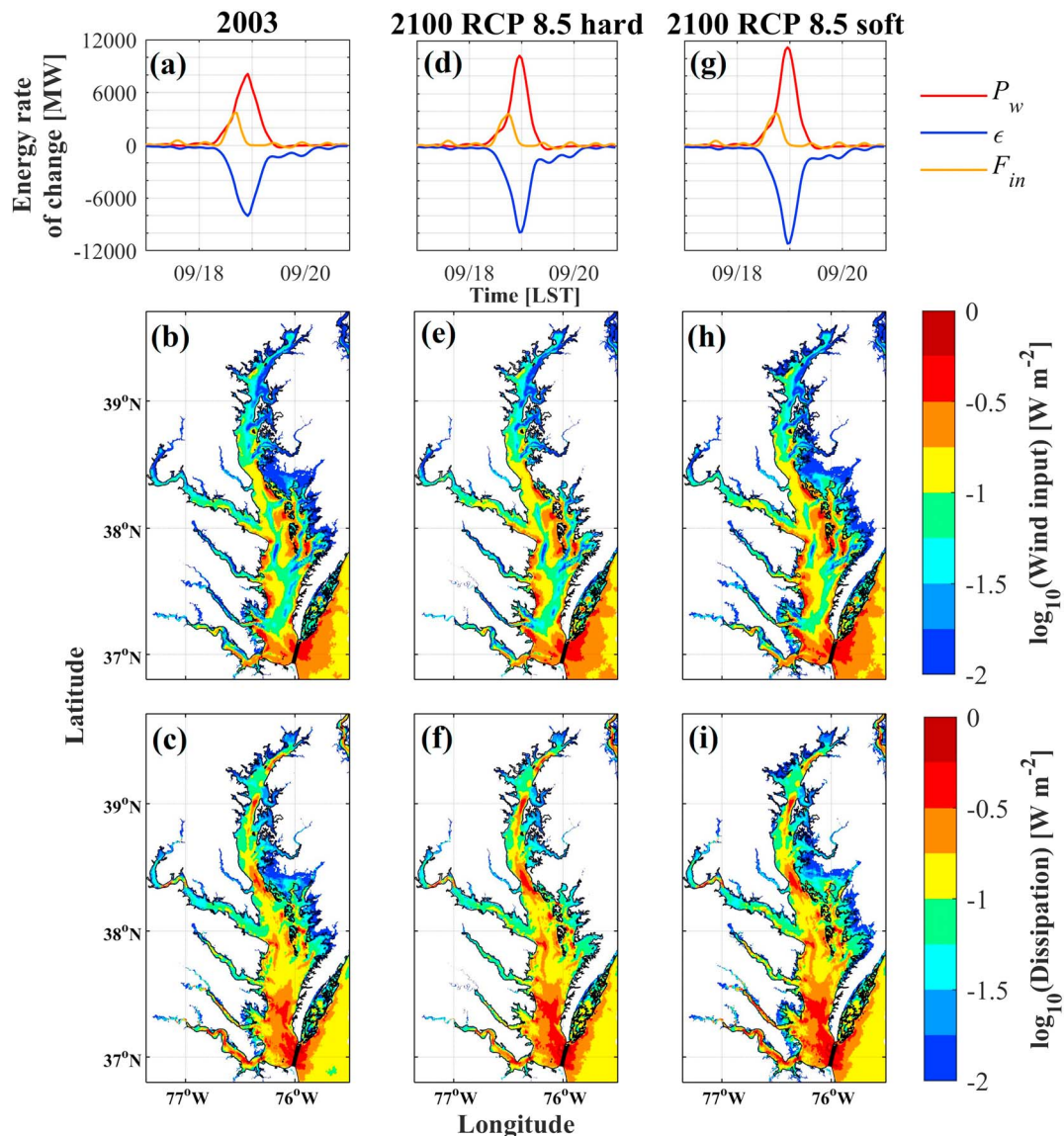
Figure 9. (a) Time series of wind energy input (P_w), energy dissipation (ε), and incoming flux (F_{in}) for hindcast of Hurricane Isabel. Spatial distribution of time-averaged (b) P_w and (c) ε over the period between 17 and 21 September for hindcast. (d and e and g–i) The same as (a)–(c) but for 2100 RCP 8.5 hard and 2100 RCP 8.5 soft scenarios, respectively. The control volume (V) is bounded by the current coastline (thin black line) and bay mouth cross section (thick black line). RCP = Representative Concentration Pathway.

exhausted and the wind energy input decreases while the energy of the storm surge currents is dissipated (Figure 10c). In the scenario of hard shoreline, no energy is leaked through the lateral boundary such that F_{lat} is exactly 0. The integrated storm surge energy reaches a higher magnitude (99 TJ) than during Hurricane Isabel (83 TJ; cf. Figures 10b and 10d). This is consistent with the results that the storm surge height is greatly amplified in the future climate and in the presence of hard shoreline, as shown in Figures 4 and 5.

Third, we investigate the energy budget for the storm in the median projection of RCP 8.5 in 2100 but with the soft shoreline. Similar to the other two scenarios, the first-order balance is still among wind energy input, incoming energy flux, and energy dissipation (Figure 9g). It is worth noting that the incoming energy flux for both storms in 2100 is larger than that during Isabel. This is expected because stronger winds in the future climate generate stronger storm surge on the shelf which subsequently propagates into the estuary. Once again, the time-averaged dissipation is greater than the local wind input in the lower Bay due to the
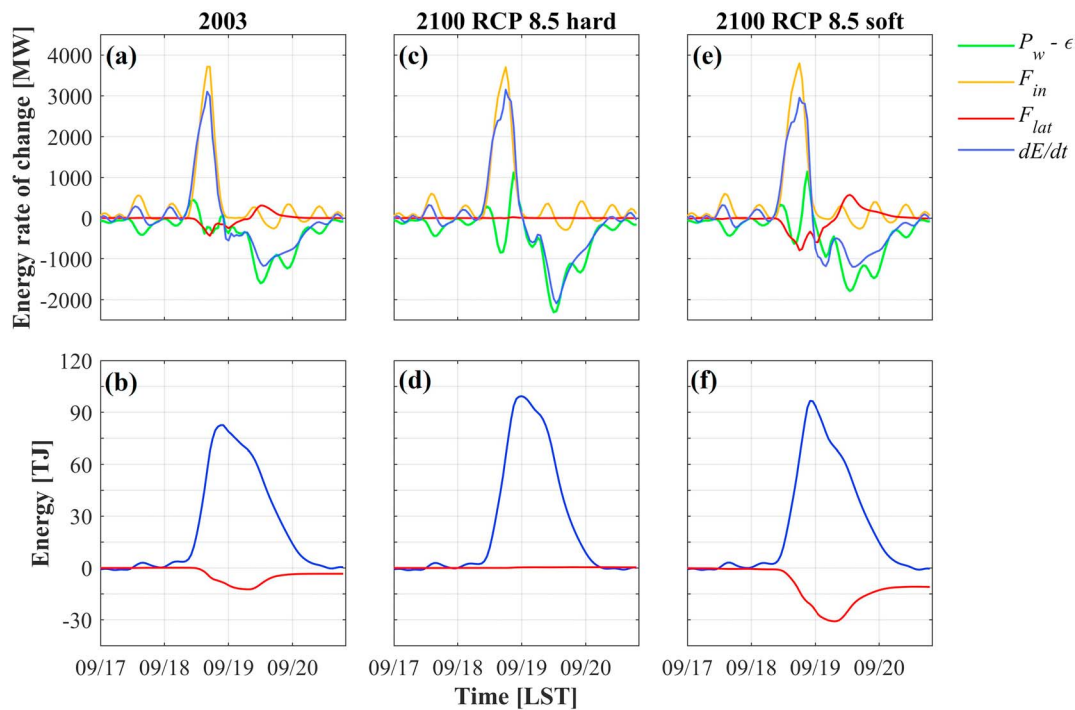
Figure 10. (a) Time series of each term in the energy budget equation and (b) accumulated dE/dt (blue) and F_{lat} (red) for the hindcast of Hurricane Isabel. (c and d and e and (f) The same as (a) and (b) but for 2100 RCP 8.5 hard and 2100 RCP 8.5 soft scenarios, respectively. 1 MW = 10^6 W and 1 TJ = 10^{12} J. RCP = Representative Concentration Pathway

incoming storm surge (Figures 9h and 9i). Compared with the hard shoreline, both the wind energy input and dissipation extend over to the newly flooded land areas but are nearly balanced there, suggesting that the storm surge energy is quickly dissipated in those shallow areas. In the second-order energy balance, the lateral energy flux is a significantly larger term as compared to that for Hurricane Isabel (Figure 10e). During the first half of the storm period, storm surge energy leaks out of the lateral boundary as the surge water floods the low-lying land areas. Later the water retreats back to the Bay, resulting in an energy influx to the control volume. Only ~65% of F_{lat} returns to the Bay, suggesting that ~35% is lost in the flooded area. Therefore, the flooded area is not only a temporary reservoir for storing storm surge energy but also dissipates energy due to bottom friction. The time series of the total energy increases to a maximum of 96 TJ, which is larger than that during Hurricane Isabel but is smaller than that for the storm with the hard shoreline (Figure 10f). This result is consistent with the differences in the storm surge heights among the three runs, as shown in Figures 4 and 5. Most interestingly, the integrated lateral energy loss reached a peak magnitude of 31 TJ, which is about 1/3 of the peak storm surge energy. This demonstrates that the lateral energy loss through flooding the low-lying areas can serve as a sizeable sink for the storm surge energy, thereby reducing storm surge height at locations further upstream. In contrast, storm surge energy is forced to propagate upstream in the presence of the hard shoreline, resulting in larger storm surge height.

6. Conclusion

Using the climate model projections to drive regional atmosphere-ocean models, we have investigated how ocean warming, sea level rise, and coastline management affect storm surge in the semienclosed Chesapeake Bay. Warming ocean produces more intense storms and stronger winds, resulting in higher storm surge. The storm surge at Norfolk rose to a maximum of 1.88 m during Hurricane Isabel. By 2100, it is projected to rise to 1.97–2.03 m under RCP 4.5 and 2.02–2.22 m under RCP 8.5, in addition to the increase in the mean sea level. Similar amplification of the storm surge is seen at Baltimore: increasing from a peak height of 2.24 m during Isabel to 2.25–2.34/2.32–2.44 m under RCP 4.5/8.5. Hardening shorelines will further raise the peak surge height in Baltimore to 2.59–2.81/2.76–3.04 m under RCP 4.5/8.5.

While sea level rise will add to the total water level, it only has a moderate effect on the storm surge height itself. Ocean warming is the main driver of stronger storm surge in the future climate. The amplification of the storm surge can reach up to 0.3 m by 2100, nearly one third of the projected sea level rise. We also found major differences in the storm surge response between the soft and hard shorelines. Hardening shorelines can further amplify the storm surge by over 0.4 m in the middle and upper parts of Chesapeake Bay. Energy budget analysis shows that allowing flooding to low-lying land leads to a significant energy loss and reduces storm surge height in the upper parts of the estuary.

It is challenging to manage coastal inundation risk in Chesapeake Bay due to its long and convoluted coastlines. Significant amount of low-lying coastal plains is located on the rural part of Eastern Shore Maryland, which is covered by extensive forests and wetlands. On the other hand, most densely populated cities (e.g., Baltimore, Washington, DC, and Annapolis), where storm surge can affect much larger population and cause more significant economic loss, are located in the upper portion of the Bay. Given the large difference in the storm surge height between the soft and hard shorelines, coastal communities around Chesapeake Bay need to explore different mitigation and adaptation strategies to deal with coastal inundation. For example, allowing for low-lying areas to be flooded and assisting the affected coastal communities in elevating their houses and/or migrating to higher grounds could significantly reduce the storm surge at the metropolitan cities located further upstream.

There are caveats worth considerations when applying these model results to coastal planning. Studies based on coarse-resolution GCMs have generally agreed on a tendency toward decreasing frequency and increasing intensity of tropical cyclones as the climate warms (Bengtsson et al., 1996). On the other hand, a consensus of GCMs predicts increasing wind shear over the North Atlantic with warming (Vecchi & Soden, 2007), which would tend to inhibit overall tropical cyclone activity. Our modeling study only considered the effect of thermodynamic component of climate change and did not consider changes in the upper wind shear. Neither did we consider the effects of surface wake cooling which could be important for a slow moving storm. Another caveat is that this paper only considered one storm (Hurricane Isabel) and its variants in the future climate. A comprehensive assessment of coastal inundation risks would require simulations of storms with different tracks and intensities.

References

Beardsley, R. C., Chen, C., & Xu, Q. (2013). Coastal flooding in Scituate (MA): A FVCOM study of the 27 December 2010 nor'easter. *Journal of Geophysical Research: Oceans*, *118*, 6030–6045. https://doi.org/10.1002/2013JC008862

Bengtsson, L., Botzet, M., & Esch, M. (1996). Will greenhouse gas-induced warming over the next 50 years lead to higher frequency and greater intensity of hurricanes? *Tellus A*, *48*(1), 57–73. https://doi.org/10.3402/tellusa.v48i1.11632

Bengtsson, L., Hodges, K. I., Esch, M., Keenlyside, N., Kornblueh, L., Luo, J. J., & Yamagata, T. (2007). How may tropical cyclones change in a warmer climate? *Tellus A: Dynamic Meteorology and Oceanography*, *59*, 539–561. https://doi.org/10.1111/j.1600-0870.2007.00251.x

Bilskie, M. V., Hagen, S. C., Alizad, K., Medeiros, S. C., Passeri, D. L., Needham, H. F., & Cox, A. (2016). Dynamic simulation and numerical analysis of hurricane storm surge under sea level rise with geomorphologic changes along the northern Gulf of Mexico. *Earth's Future*, *4*, 177–193. https://doi.org/10.1002/2015EF000347

Boesch, D. F., Boicourt, W. C., Cullather, R. I., Ezer, T., Galloway, G. E. Jr., Johnson, Z. P., et al. (2018). *Sea-level rise: Projections for Maryland 2018* (p. 27). Cambridge, MD: University of Maryland Center for Environmental Science.

Boicourt, W. C. (2005). Physical response of Chesapeake Bay to hurricanes moving to the wrong side: Refining the forecasts. In K. G. Sellner (Ed.), *Hurricane Isabel in Perspective*, CRC Publ. 05-160, edited by, (pp. 39–48). Edgewater, MD: Chesapeake Res. Consortium.

Burchard, H. (2002). *Applied turbulence modelling in marine waters*. Berlin, Germany: Springer. https://doi.org/10.1007/3-540-45419-5

Chen, C., Beardsley, R. C., & Cowles, G. (2006). An unstructured grid, finite-volume coastal ocean model (FVCOM) system. *Oceanography*, *19*(1), 78–89. https://doi.org/10.5670/oceanog.2006.92

Chen, C., Beardsley, R. C., Luettich, R. A. Jr., Westerink, J. J., Wang, H., Perrie, W., et al. (2013). Extratropical storm inundation testbed: Intermodel comparisons in Scituate, Massachusetts. *Journal of Geophysical Research: Oceans*, *118*, 5054–5073. https://doi.org/10.1002/jgrc.20397

Chen, C., Liu, H., & Beardsley, R. C. (2003). An unstructured grid, finite-volume, three-dimensional, primitive equations ocean model: Application to coastal ocean and estuaries. *Journal of Atmospheric and Oceanic Technology*, *20*(1), 159–186. https://doi.org/10.1175/1520-0426(2003)020<0159:AUGFVT>2.0.CO;2

Chen, C., Beardsley, R., ., Cowles, G., Qi, J., Lai, Z., Gao, G., et al. (2011). *An unstructured-grid, finite-volume community ocean model fvcom user manual*, SMAST/UMASSD-11-1101, (3rd ed. p. 315).

Church, J. A., Clark, P. U., Cazenave, A., Gregory, J. M., Jevrejeva, S., Levermann, A., et al. (2013). Sea level change. In T. F. Stocker, D. Qin, G.-K. Plattner, M. Tignor, S. K. Allen, J. Boschung, A. Nauels, Y. Xia, V. Bex, & P. M. Midgley (Eds.), *Climate change 2013: The physical science basis contribution of Working Group I to the Fifth Assessment Report of the Intergovernmental Panel on Climate Change* (pp. 1137–1216). U. K.: Cambridge University Press.

Cummins, P. F., & Oey, L. Y. (1997). Simulation of barotropic and baroclinic tides off northern British Columbia. *Journal of Physical Oceanography*, *27*(5), 762–781. https://doi.org/10.1175/1520-0485(1997)027<0762:SOBABT>2.0.CO;2

Domingues, C. M., Church, J. A., White, N. J., Gleckler, P. J., Wijffels, S. E., Barker, P. M., & Dunn, J. R. (2008). Improved estimates of upper-ocean warming and multi-decadal sea-level rise. *Nature*, *453*(7198), 1090–1093. https://doi.org/10.1038/nature07080

Domingues, C. M., Goni, G., Baringer, M., & Volkov, D. (2018). What caused the accelerated sea level changes along the U.S. East Coast during 2010–2015? *Geophysical Research Letters*, *45*, 13,367–13,376. https://doi.org/10.1029/2018GL081183

Egbert, G. D., & Erofeeva, S. Y. (2002). Efficient inverse modeling of barotropic ocean tides. *Journal of Atmospheric and Oceanic Technology*, *19*(2), 183–204. https://doi.org/10.1175/1520-0426(2002)019<0183:EIMOBO>2.0.CO;2

Eichler, T. P., Gaggini, N., & Pan, Z. (2013). Impacts of global warming on Northern Hemisphere winter storm tracks in the CMIP5 model suite. *Journal of Geophysical Research: Atmospheres*, *118*, 3919–3932. https://doi.org/10.1002/jgrd.50286

Emanuel, K., Sundararajan, R., & Williams, J. (2008). Hurricanes and global warming: Results from downscaling IPCC AR4 simulations. *Bulletin of the American Meteorological Society*, *89*(3), 347–368. https://doi.org/10.1175/BAMS-89-3-347

Emanuel, K. A. (2013). Downscaling CMIP5 climate models shows increased tropical cyclone activity over the 21st century. *Proceedings of the National Academy of Sciences*, *110*(30), 12,219–12,224. https://doi.org/10.1073/pnas.1301293110

Ezer, T. (2013). Sea level rise, spatially uneven and temporally unsteady: Why the US East Coast, the global tide gauge record, and the global altimeter data show different trends. *Geophysical Research Letters*, *40*, 5439–5444. https://doi.org/10.1002/2013GL057952

Ezer, T., Atkinson, L. P., Corlett, W. B., & Blanco, J. L. (2013). Gulf Stream's induced sea level rise and variability along the US mid-Atlantic coast. *Journal of Geophysical Research: Oceans*, *118*, 685–697. https://doi.org/10.1002/jgrc.20091

Fairall, C. W., Bradley, E. F., Hare, J. E., Grachev, A. A., & Edson, J. B. (2003). Bulk parameterization of air–sea fluxes: Updates and verification for the COARE algorithm. *Journal of Climate*, *16*(4), 571–591. https://doi.org/10.1175/1520-0442(2003)016<0571:BPOASF>2.0.CO;2

Gill, A. E. (1982). *Atmosphere–ocean dynamics* (p. 662). New York: Academic Press.

Hill, K. A., & Lackmann, G. M. (2011). The impact of future climate change on TC intensity and structure: A downscaling approach. *Journal of Climate*, *24*(17), 4644–4661. https://doi.org/10.1175/2011JCLI3761.1

Holleman, R. C., & Stacey, M. T. (2014). Coupling of sea level rise, tidal amplification, and inundation. *Journal of Physical Oceanography*, *44*(5), 1439–1455.

Hong, S. Y., Noh, Y., & Dudhia, J. (2006). A new vertical diffusion package with an explicit treatment of entrainment processes. *Monthly Weather Review*, *134*(9), 2318–2341. https://doi.org/10.1175/MWR3199.1

Iacono, M. J., Delamere, J. S., Mlawer, E. J., Shephard, M. W., Clough, S. A., & Collins, W. D. (2008). Radiative forcing by long-lived greenhouse gases: Calculations with the AER radiative transfer models. *Journal of Geophysical Research*, *113*, D13103. https://doi.org/10.1029/2008JD009944

IPCC (2013). Climate change 2013: The physical science basis. Working Group I Contribution to the IPCC 5th Assessment Report - Changes to the Underlying Scientific/Technical Assessment (IPCC-XXVI/Doc.4).

Kain, J. S. (2004). The Kain–Fritsch convective parameterization: An update. *Journal of Applied Meteorology*, *43*(1), 170–181. https://doi.org/10.1175/1520-0450(2004)043<0170:TKCPAU>2.0.CO;2

Knutson, T. R., Sirutis, J. J., Vecchi, G. A., Garner, S., Zhao, M., Kim, H. S., et al. (2013). Dynamical downscaling projections of twenty-first-century Atlantic hurricane activity: CMIP3 and CMIP5 model-based scenarios. *Journal of Climate*, *26*(17), 6591–6617. https://doi.org/10.1175/JCLI-D-12-00539.1

Knutson, T. R., & Tuleya, R. E. (2004). Impact of CO_2-induced warming on simulated hurricane intensity and precipitation: Sensitivity to the choice of climate model and convective parameterization. *Journal of Climate*, *17*(18), 3477–3495. https://doi.org/10.1175/1520-0442(2004)017<3477:IOCWOS>2.0.CO;2

Knutson, T. R., & Tuleya, R. E. (2008). *Tropical cyclones and climate change: Revisiting recent studies at GFDL*, (pp. 120–144). Cambridge, UK: Cambridge University Press.

Kopp, R. E., DeConto, R. M., Bader, D. A., Hay, C. C., Horton, R. M., Kulp, S., et al. (2017). Evolving understanding of Antarctic ice-sheet physics and ambiguity in probabilistic sea-level projections. *Earth's Future*, *5*, 1217–1233. https://doi.org/10.1002/2017EF000663

Kopp, R. E., Horton, R. M., Little, C. M., Mitrovica, J. X., Oppenheimer, M., Rasmussen, D. J., et al. (2014). Probabilistic 21st and 22nd century sea-level projections at a global network of tide-gauge sites. *Earth's future*, *2*, 383–406. https://doi.org/10.1002/2014EF000239

Lee, S. B., Li, M., & Zhang, F. (2017). Impact of sea level rise on tidal range in Chesapeake and Delaware Bays. *Journal of Geophysical Research: Oceans*, *122*, 3917–3938. https://doi.org/10.1002/2016JC012597

Li, M., Zhong, L., Boicourt, W. C., Zhang, S., & Zhang, D. L. (2006). Hurricane-induced storm surges, currents and destratification in a semi-enclosed bay. *Geophysical Research Letters*, *33*, L02604. https://doi.org/10.1029/2005GL024992

Li, M., Zhong, L., Boicourt, W. C., Zhang, S., & Zhang, D. L. (2007). Hurricane-induced destratification and restratification in a partially-mixed estuary. *Journal of Marine Research*, *65*(2), 169–192. https://doi.org/10.1357/002224007780882550

Li, X., & Pu, Z. (2008). Sensitivity of numerical simulation of early rapid intensification of Hurricane Emily (2005) to cloud microphysical and planetary boundary layer parameterizations. *Monthly Weather Review*, *136*(12), 4819–4838. https://doi.org/10.1175/2008MWR2366.1

Lin, N., Emanuel, K., Oppenheimer, M., & Vanmarcke, E. (2012). Physically based assessment of hurricane surge threat under climate change. *Nature Climate Change*, *2*(6), 462–467. https://doi.org/10.1038/nclimate1389

Lin, N., Kopp, R. E., Horton, B. P., & Donnelly, J. P. (2016). Hurricane Sandy's flood frequency increasing from year 1800 to 2100. *Proceedings of the National Academy of Sciences*, *113*(43), 12,071–12,075. https://doi.org/10.1073/pnas.1604386113

Mallard, M. S., Lackmann, G. M., Aiyyer, A., & Hill, K. (2013). Atlantic hurricanes and climate change. Part I: Experimental design and isolation of thermodynamic effects. *Journal of Climate*, *26*(13), 4876–4893. https://doi.org/10.1175/JCLI-D-12-00182.1

Miller, K. G., Kopp, R. E., Horton, B. P., Browning, J. V., & Kemp, A. C. (2013). A geological perspective on sea-level rise and its impacts along the US mid-Atlantic coast. *Earth's Future*, *1*, 3–18. https://doi.org/10.1002/2013EF000135

Moss, R. H., Edmonds, J. A., Hibbard, K. A., Manning, M. R., Rose, S. K., van Vuuren, D. P., et al. (2010). The next generation of scenarios for climate change research and assessment. *Nature*, *463*(7282), 747–756. https://doi.org/10.1038/nature08823

Mousavi, M. E., Irish, J. L., Frey, A. E., Olivera, F., & Edge, B. L. (2011). Global warming and hurricanes: the potential impact of hurricane intensification and sea level rise on coastal flooding. *Climatic Change*, *104*(3-4), 575–597.

Nolan, D. S., Stern, D. P., & Zhang, J. A. (2009). Evaluation of planetary boundary layer parameterizations in tropical cyclones by comparison of in situ observations and high-resolution simulations of Hurricane Isabel (2003). Part II: Inner-core boundary layer and eye-wall structure. *Monthly Weather Review*, *137*(11), 3675–3698.

Nolan, D. S., Zhang, J. A., & Stern, D. P. (2009). Evaluation of planetary boundary layer parameterizations in tropical cyclones by comparison of in situ observations and high-resolution simulations of Hurricane Isabel (2003). Part I: Initialization, maximum winds, and the outer-core boundary layer. *Monthly Weather Review*, *137*(11), 3651–3674.

Pelling, H. E., Uehara, K., & Green, J. A. M. (2013). The impact of rapid coastline changes and sea level rise on the tides in the Bohai Sea, China. *Journal of Geophysical Research: Oceans*, *118*, 3462–3472. https://doi.org/10.1002/jgrc.20258

Pickering, M. D., Wells, N. C., Horsburgh, K. J., & Green, J. A. M. (2012). The impact of future sea-level rise on the European Shelf tides. *Continental Shelf Research*, *35*, 1–15. https://doi.org/10.1016/j.csr.2011.11.011

Sallenger, A. H. Jr., Doran, K. S., & Howd, P. A. (2012). Hotspot of accelerated sea-level rise on the Atlantic coast of North America. *Nature Climate Change*, *2*(12), 884.

Seroka, G., Miles, T., Xu, Y., Kohut, J., Schofield, O., & Glenn, S. (2016). Hurricane Irene sensitivity to stratified coastal ocean cooling. *Monthly Weather Review*, *144*(9), 3507–3530. https://doi.org/10.1175/MWR-D-15-0452.1

Shen, J., Wang, H., Sisson, M., & Gong, W. (2006). Storm tide simulation in the Chesapeake Bay using an unstructured grid model. *Estuarine, Coastal and Shelf Science*, *68*(1-2), 1–16. https://doi.org/10.1016/j.ecss.2005.12.018

Shen, W., Tuleya, R. E., & Ginis, I. (2000). A sensitivity study of the thermodynamic environment on GFDL model hurricane intensity: Implications for global warming. *Journal of Climate*, *13*(1), 109–121. https://doi.org/10.1175/1520-0442(2000)013<0109:ASSOTT>2.0.CO;2

Skamarock, W. C., Klemp, J. B., Dudhia, J., Gill, D. O., Barker, D. M., Duda, M. G., et al. (2008). A Description of the Advanced Research WRF Version 3. NCAR Technical Note NCAR/TN-475+ STR.

Smith, J. M., Cialone, M. A., Wamsley, T. V., & McAlpin, T. O. (2010). Potential impact of sea level rise on coastal surges in southeast Louisiana. *Ocean Engineering*, *37*(1), 37–47. https://doi.org/10.1016/j.oceaneng.2009.07.008

Thompson, G., Field, P. R., Rasmussen, R. M., & Hall, W. D. (2008). Explicit forecasts of winter precipitation using an improved bulk microphysics scheme. Part II: Implementation of a new snow parameterization. *Monthly Weather Review*, *136*(12), 5095–5115. https://doi.org/10.1175/2008MWR2387.1

Tuleya, R. E., Bender, M., Knutson, T. R., Sirutis, J. J., Thomas, B., & Ginis, I. (2016). Impact of upper-tropospheric temperature anomalies and vertical wind shear on tropical cyclone evolution using an idealized version of the operational GFDL hurricane model. *Journal of the Atmospheric Sciences*, *73*(10), 3803–3820. https://doi.org/10.1175/JAS-D-16-0045.1

Van Vuuren, D. P., Edmonds, J., Kainuma, M., Riahi, K., Thomson, A., Hibbard, K., et al. (2011). The representative concentration pathways: An overview. *Climatic Change*, *109*(1-2), 5–31. https://doi.org/10.1007/s10584-011-0148-z

Vecchi, G. A., & Soden, B. J. (2007). Increased tropical Atlantic wind shear in model projections of global warming. *Geophysical Research Letters*, *34*, L08702. https://doi.org/10.1029/2006GL028905

Wang, R. Q., Herdman, L. M., Erikson, L., Barnard, P., Hummel, M., & Stacey, M. T. (2017). Interactions of estuarine shoreline infrastructure with multiscale sea level variability. *Journal of Geophysical Research: Oceans*, *122*, 9962–9979. https://doi.org/10.1002/2017JC012730

Ward, S. L., Green, J. M., & Pelling, H. E. (2012). Tides, sea-level rise and tidal power extraction on the European shelf. *Ocean Dynamics*, *62*(8), 1153–1167. https://doi.org/10.1007/s10236-012-0552-6

Warner, J. C., Sherwood, C. R., Arango, H. G., & Signell, R. P. (2005). Performance of four turbulence closure models implemented using a generic length scale method. *Ocean Modelling*, *8*(1-2), 81–113. https://doi.org/10.1016/j.ocemod.2003.12.003

Weisberg, R. H., & Zheng, L. (2006). Hurricane storm surge simulations for Tampa Bay. *Estuaries and Coasts*, *29*(6), 899–913. https://doi.org/10.1007/BF02798649

Woollings, T., Gregory, J. M., Pinto, J. G., Reyers, M., & Brayshaw, D. J. (2012). Response of the North Atlantic storm track to climate change shaped by ocean–atmosphere coupling. *Nature Geoscience*, *5*(5), 313.

Yang, Z., Wang, T., Leung, R., Hibbard, K., Janetos, T., Kraucunas, I., et al. (2014). A modeling study of coastal inundation induced by storm surge, sea-level rise, and subsidence in the Gulf of Mexico. *Natural Hazards*, *71*(3), 1771–1794. https://doi.org/10.1007/s11069-013-0974-6

Yin, J., Schlesinger, M. E., & Stouffer, R. J. (2009). Model projections of rapid sea-level rise on the northeast coast of the United States. *Nature Geoscience*, *2*(4), 262.

Zervas, C. (2001). Sea level variations of the United States 1854-1999. *NOAA Technical Report NOS CO-OPS, 36*, 187 pp., Natl. Oceanic and Atmos. Admin., Silver Spring, Md.

Zervas, C. (2009). Sea level variations of the United States 1854–2006. *NOAA Technical Report NOS CO-OPS*, *53*, 176 pp., Natl. Oceanic and Atmos. Admin., Silver Spring, Md.

Zhang, F., Li, M., Ross, A. C., Lee, S. B., & Zhang, D. L. (2017). Sensitivity analysis of Hurricane Arthur (2014) storm surge forecasts to WRF physics parameterizations and model configurations. *Weather and Forecasting*, *32*(5), 1745–1764. https://doi.org/10.1175/WAF-D-16-0218.1

Zhong, L., & Li, M. (2006). Tidal energy fluxes and dissipation in the Chesapeake Bay. *Continental Shelf Research*, *26*(6), 752–770. https://doi.org/10.1016/j.csr.2006.02.006

Zhong, L., Li, M., & Zhang, D. L. (2010). How do uncertainties in hurricane model forecasts affect storm surge predictions in a semi-enclosed bay? *Estuarine, Coastal and Shelf Science*, *90*(2), 61–72. https://doi.org/10.1016/j.ecss.2010.07.001